

# Disentangling the stellar populations in the counter-rotating disc galaxy NGC 4550

Evelyn J. Johnston,<sup>1\*</sup> Michael R. Merrifield,<sup>1</sup> Alfonso Aragón-Salamanca<sup>1</sup> and Michele Cappellari<sup>2</sup>

<sup>1</sup>*School of Physics and Astronomy, University of Nottingham, University Park, Nottingham, NG7 2RD, UK*

<sup>2</sup>*Sub-department of Astrophysics, Department of Physics, University of Oxford, Denys Wilkinson Building, Keble Road, Oxford, OX1 3RH, UK*

3 October 2012

## ABSTRACT

In order to try and understand its origins, we present high-quality long-slit spectral observations of the counter-rotating stellar discs in the strange S0 galaxy NGC 4550. We kinematically decompose the spectra into two counter-rotating stellar components (plus a gaseous component), in order to study both their kinematics and their populations. The derived kinematics largely confirm what was known previously about the stellar discs, but trace them to larger radii with smaller errors; the fitted gaseous component allows us to trace the hydrogen emission lines for the first time, which are found to follow the same rather strange kinematics previously seen in the [OIII] line. Analysis of the populations of the two separate stellar components shows that the secondary disc has a significantly younger mean age than the primary disc, consistent with later star formation from the associated gaseous material. In addition, the secondary disc is somewhat brighter, also consistent with such additional star formation. However, these measurements cannot be self-consistently modelled by a scenario in which extra stars have been added to initially-identical counter-rotating stellar discs, which rules out Evans & Collett’s (1994) elegant “separatrix-crossing” model for the formation of such massive counter-rotating discs from a single galaxy, leaving some form of unusual gas accretion history as the most likely formation mechanism.

**Key words:** galaxies: elliptical and lenticular – galaxies: evolution – galaxies: formation – galaxies: individual (NGC 4550) – galaxies: kinematics and dynamics – galaxies: stellar content

## 1 INTRODUCTION

The presence of counter-rotating populations of stars in S0 galaxies is a well-known phenomenon, although reasonably uncommon: while almost a quarter of S0 galaxies contain gaseous components that counter-rotate relative to their stars, less than 10% were found to contain distinct counter-rotating stellar disc components (Bertola, Buson & Zeilinger 1992; Kuijken, Fisher & Merrifield 1996). However, such systems do exist, and so any theory of S0 formation must provide a channel for their creation.

Of these counter-rotating systems, the one that presents the greatest challenge to models of galaxy formation is NGC 4550. Rubin, Graham & Kenney (1992) obtained long-slit spectra along the major axis of this normal-looking S0 galaxy, and found that the absorption-lines split neatly into two, indicating two extended counter-rotating discs. Subsequent analysis has confirmed that these discs are very similar, with comparable sizes, masses, kinematics and line strength (Rix et al. 1992). Integral-field observations, in combination with dynamical models, confirmed the pic-

ture, but revealed some breaking of the symmetry, with one disc being thicker than the other (Cappellari et al. 2007) and also containing an emission-lines component (Sarzi et al. 2006).

The reason that it is difficult to come up with a scenario for constructing such a system is that the obvious solution of merging two normal discs with opposite angular momenta does not generally work. In particular, it has long been known that most mergers between two roughly equally-massive discs are likely to be very destructive, heating the system enormously and not resulting in the required disc-like final morphology (Toomre 1977). However, this problem may not be insurmountable: Puerari & Pfenniger (2001) show that a major merger between disc galaxies of comparable mass could produce the kinematics seen in NGC 4550, as long as the initial conditions are just right, with the precursor systems co-planar on a carefully-chosen parabolic orbit. A similar result was found by (Crocker et al. 2009), who also tried to reproduce the gas kinematics of the galaxy. Clearly, such an arrangement is rather contrived, but not impossible if systems like NGC 4550 are truly rare. The ATLAS<sup>3D</sup> survey (Cappellari et al. 2011) obtained integral field stellar kinematics for a volume-limited sample of 260 early-type galaxies. Out of these they found 11 cases (see fig. C5 of

\* Email: ppexj@nottingham.ac.uk

Krajnović et al. 2011) showing evidence for major counter-rotating stellar discs. However in only about half of these (about 2% of the sample) the two counter-rotating discs seem to have comparable mass like NGC 4550.

An alternative scenario that avoids the destructive force of a major merger is the possibility that counter-rotating gas could be accreted rather slowly by a normal disc galaxy, and subsequently form stars in a new counter-rotating disc. This possibility was explored through simulations by Thakar & Ryden (1996, 1998), who found that the counter-rotating stellar disc formed in this way tended to be rather small. They did find that a series of mergers with gas-rich dwarf galaxies could produce a counter-rotating disc of comparable mass and size to the original, but once again the initial conditions needed to be very carefully tuned to produce such matched discs.

The similarity of the two discs in NGC 4550 led Evans & Collett (1994) to suggest a third possibility that could much more naturally produce identical counter-rotating discs. In this “separatrix-crossing” scenario, a single initially-triaxial elliptical galaxy evolves slowly with time into an axisymmetric morphology. At that point, the family of box orbits that existed in the triaxial system would disappear, and stars would switch onto tube orbits instead. Since the initial box orbit had no preferred sense of rotation, stars would end up randomly on tube orbits rotating in either sense around the centre of the now-axisymmetric system, thus automatically generating a pair of identical counter-rotating stellar populations.

To-date, it has not been clear which, if any, of these scenarios might be responsible for the formation of NGC 4550. However, they do predict some distinct difference in the resulting counter-rotating discs, particularly in the properties of their stellar populations, which we might be able to use to distinguish between them. While the separatrix-crossing scenario will produce truly identical discs, a counter-rotating stellar disc formed by gas accretion must have a younger population than the pre-existing disc, while the counter-rotating discs in a system formed by a merger will reflect the stellar populations of the progenitor galaxies.

In this paper, we set out to analyse simultaneously the kinematics and stellar populations of NGC 4550, to try to distinguish between these possibilities. The remainder of the paper is laid out as follows: Section 2 describes the new spectral data we have used; in Section 3, we present the fitting technique developed to separate out the stellar component, and present the resulting kinematic measurements; Section 4 analyses the individual component spectra to quantify their populations; and Section 5 discusses the implications of these measurements for the various theories as to how this galaxy might have formed.

## 2 OBSERVATIONS AND DATA REDUCTION

The requisite spectral observations along the major axis of NGC 4550 were carried out using the GMOS instruments in long-slit mode on Gemini-North and Gemini-South on 2009 June 20 and 2010 February 13 respectively. 1800 seconds of exposure was obtained with each telescope. Spatially, the chips were binned by 4, to give a final scale of  $0.29 \text{ arcseconds pixel}^{-1}$ . The measured seeing of  $\sim 1.77 \text{ arcsec}$  with Gemini-South and  $\sim 0.9 \text{ arcsec}$  with Gemini-North was well below the spatial scales of interest in this extended system – adopting a distance of  $15.5 \text{ Mpc}$  to this galaxy (Mei et al. 2007),  $1 \text{ arcsec} \equiv 75 \text{ pc}$ . We used a  $0.5 \text{ arcsecond}$  slit and the B1200 grating, with a central wavelength of  $\sim 4730 \text{ \AA}$ ,

**Table 1.** Spectrophotometric (S) and template (T) stars.

Name	T/S	Spectral Class
HD054719	T	K2 III
HD070272	T	K5 III
HD072324	T	G9 III
HD073593	T	G8 IV
HD120136	T	F6 IV
HD144872	T	K3 V
HD145148	T	K0 IV
HD161817	T	A2 VI
Feige66	S	-
Hiltner600	S	-
LTT1788	S	-

slightly offset between the two sets of exposures to fill in the gaps between the chips. These observations thus provided an hour of integration over the spectral range  $4100 - 5450 \text{ \AA}$  with a dispersion of  $0.235 \text{ \AA pixel}^{-1}$ . The spectral resolution was measured from the FWHM of the arc lines to be  $\sim 1.13 \text{ \AA}$ , which corresponds to a velocity resolution of  $72 \text{ km s}^{-1}$  FWHM or a velocity dispersion of  $30 \text{ km s}^{-1}$ .

As part of a larger programme of observations, a series of spectrophotometric and template stars were also observed with the same instrumental set up, of which the details are given in Table 1. The template stars cover a range of spectral types in order to match the composite spectral type of the galaxy in our combined stellar kinematic and population analysis.

The science spectra, along with dome flats taken following each set of observations and CuAr arc spectra from the same instrumental set-up, were reduced using the GMOS spectral reduction packages in IRAF.<sup>1</sup> All the science and calibration frames were reduced by applying bias subtraction, flat fielding, cosmic ray removal and an initial wavelength calibration, and the three sections of each spectrum from each CCD were joined together. The arc spectra were then used to correct for the geometric distortions caused by the instrument optics and to refine the wavelength solution over the whole spectrum; the residuals of the resulting wavelength fits were  $\sim 0.2 - 0.3 \text{ \AA}$ .

The wavelength-calibrated spectra were then sky subtracted, corrected for atmospheric extinction and flux calibrated using the spectrophotometric standard star spectra. Finally, the spectra from each telescope were combined, using the measured positions of prominent sky lines to ensure the best possible registration of absolute wavelength calibration. The resulting two-dimensional spectrum for the galaxy, representing an hour of integration on an 8-metre telescope, provides the very high signal-to-noise ratio required for this combined kinematic and population analysis: the central 2 arcseconds of the galaxy yield a spectrum with a signal-to-noise ratio in excess of 100, and judicious binning allows us to keep the signal-to-noise ratio in excess of 20 throughout the galaxy.

<sup>1</sup> IRAF is distributed by the National Optical Astronomy Observatories, which are operated by the Association of Universities for Research in Astronomy, Inc., under cooperative agreement with the National Science Foundation

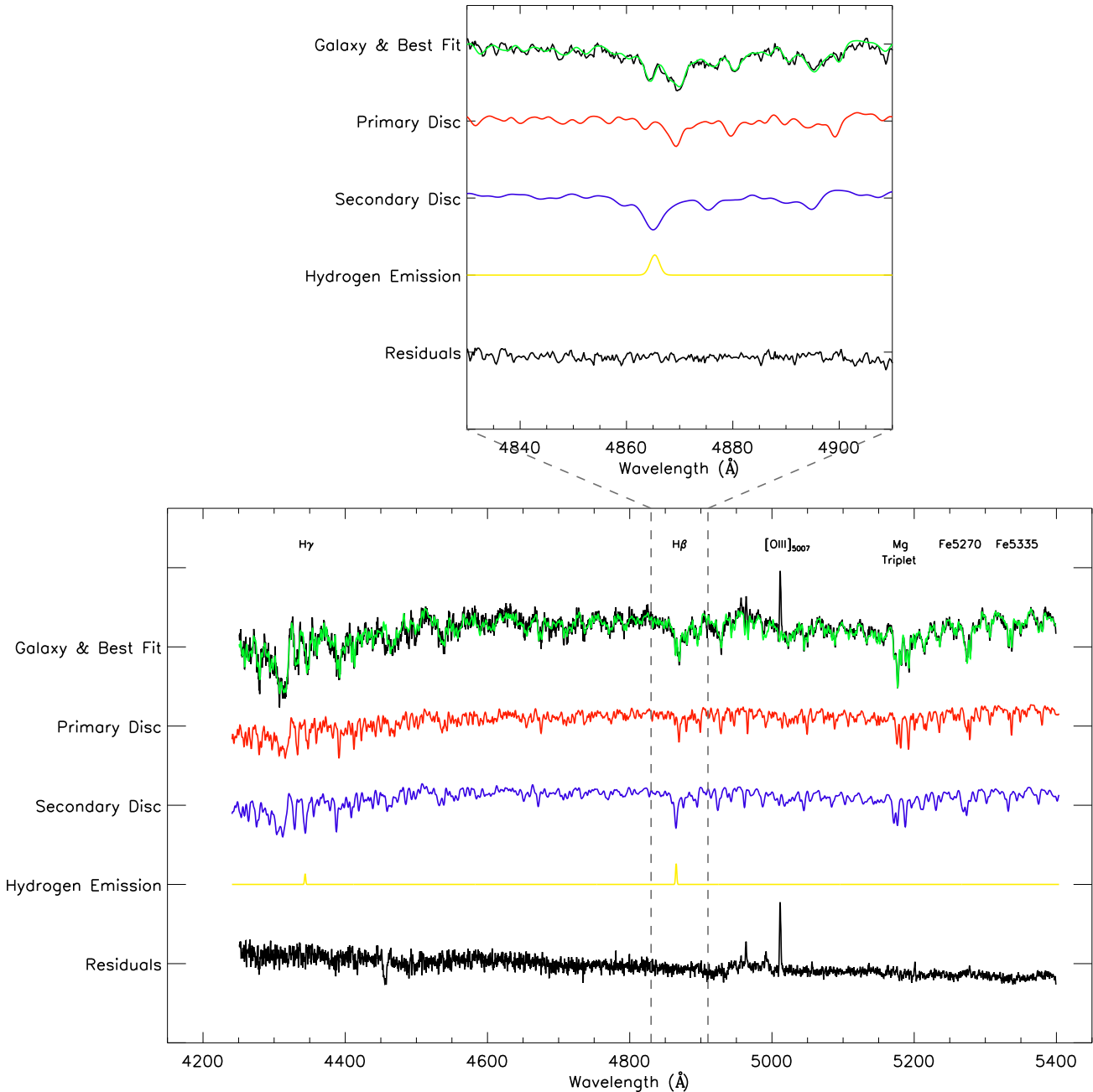


**Figure 1.** The spectrum of one side of the outer disc of NGC 4550, showing both the full spectral range and a zoom in on the  $H\beta$  line. The data are shown in black, and the green line shows the best-fit model. The individual components that comprise this model and the residuals of the fit are also shown. Note- the polynomials are not included in this fit.

### 3 KINEMATIC DECOMPOSITION

In order to study the stellar populations of the two component counter-rotating discs, we must first separate their spectra. Fortunately, outside the central few arcseconds, the line-of-sight velocities of the two components are different enough to split the corresponding absorption lines quite cleanly – indeed, it was this splitting that enabled Rubin, Graham & Kenney (1992) to identify the counter-rotating discs in the first place – so we can fit a two-component spectral model, where each component has a different mean velocity and velocity dispersion, reasonably unambiguously. At the same time, we also have to allow for the unknown stel-

lar population properties of the two components. In order to fit all these factors simultaneously, we modified the Penalized Pixel Fitting code (PPXF) of Cappellari & Emsellem (2004) in a similar way to Coccato et al. (2011). This code combines the template stars listed in Table 1 to produce two model spectra representing the two stellar population components, which when added together would best fit the galaxy spectrum. To achieve the best fit, the component spectra were multiplied by low-order Legendre polynomials to model out any mismatch in the flux calibration of the continuum, and convolved with line-of-sight velocity distributions of different

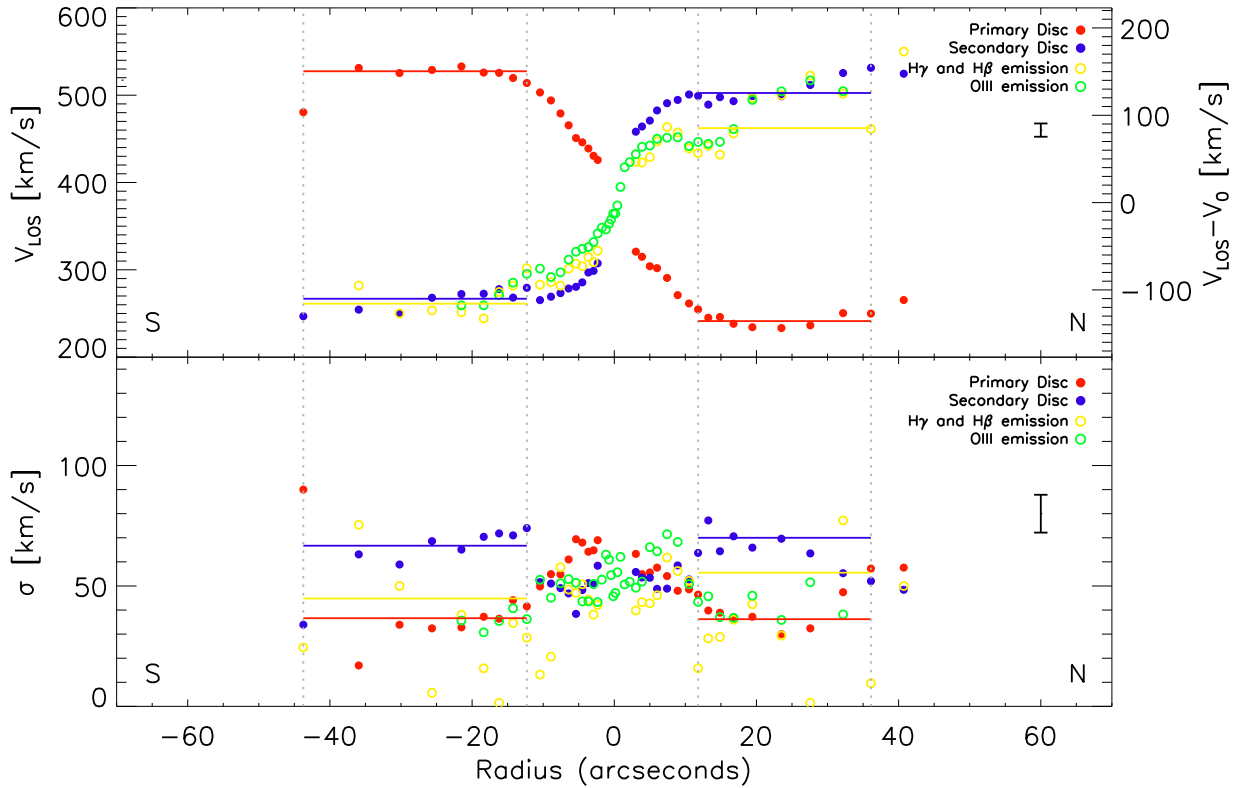


**Figure 2.** Measurements of the radial velocity and velocity dispersion for each kinematic component fitted to the spectra of NGC 4550 as a function of radial position along the major axis (with north and south directions annotated). Typical characteristic error bars are shown on the right of each plot. The horizontal lines show the results of fitting to spectra co-added over the entire flat part of the rotation curve (marked by vertical dotted lines). The kinematics of the  $[\text{OIII}]_{\lambda 5007}$  line, derived by direct fitting to the spectral line, are also shown.

shapes, mean velocities and dispersions, to best represent the kinematics of each component.

One further complication is that it is clear from the raw spectra that there is a third, gaseous, component rotating in one direction, as is evident from the strong  $[\text{OIII}]_{\lambda 5007}$  emission line. We can deal with this contaminant by simply masking it from the spectral range used in the fitting. However, there is, presumably, also emission from hydrogen gas, which usually accompanies the  $[\text{OIII}]$  line in galaxies. Such emission could prove disastrous for the analysis of this paper, as it would partially fill in the hydrogen absorption lines of one of the stellar components, completely altering the derived line strengths of these important lines, and thus the inferred properties of the stellar population. We therefore fit a third component consisting simply of two Gaussians at the wavelengths of the  $H\beta$  and  $H\gamma$  features, with a FWHM equal to the spectral resolution of the galaxy spectrum and the ratio of their intensities given by the Balmer decrement from Reynolds et al. (1997). By convolving this component with its own velocity distribution in the fit process, we also obtain the kinematics of the gas component. Fortunately, due to the long wavelength range over which the spectra are fit, and because the ratio of hydrogen emission line strengths in the gaseous component is different from the ratio of the corresponding absorption lines in the underlying stellar component, there is not a degeneracy in the resulting fit, so both components can be independently extracted. In principle, differential reddening could introduce a degeneracy problem, but because this galaxy is an S0 with little ev-

idence for large amounts of dust, the effect is not thought to be significant.

A typical result of this fitting process is illustrated in Figure 1. As well as confirming the generally very good job that this fitting process does in reproducing the full spectrum with the three components, this figure also underlines the importance of including the gas component: from the raw spectrum, one might conclude that the  $H\beta$  absorption line is somewhat stronger in the redshifted (primary disc) component, but the full fitting process reveals that this conclusion is driven by the filling in of the absorption feature in the blueshifted component by the emission line, and actually it is this secondary-disc component that has the stronger absorption line.

This fitting process was repeated using the spectral data from all along the major axis, co-added spatially to maintain a signal-to-noise ratio of at least 20 per pixel. Only the central  $\sim 5$  arcsec could not be decomposed in this way, due in combination to the overlapping kinematics of the two discs and the increasing contribution to the light from the bulge. The mean velocities and velocity dispersions derived for the three components are shown in Figure 2. Errors on each point were estimated by Monte Carlo simulations of model galaxies constructed using the same components as in the fit; for clarity, we do not plot all points with error bars, but show the mean resulting error on the right of the plot. We also tested the sensitivity of the kinematic results to the spectral templates adopted by repeating the analysis using a sub-sample of the ELODIE spectral templates (Prugniel & Soubiran 2001) that covered the full range

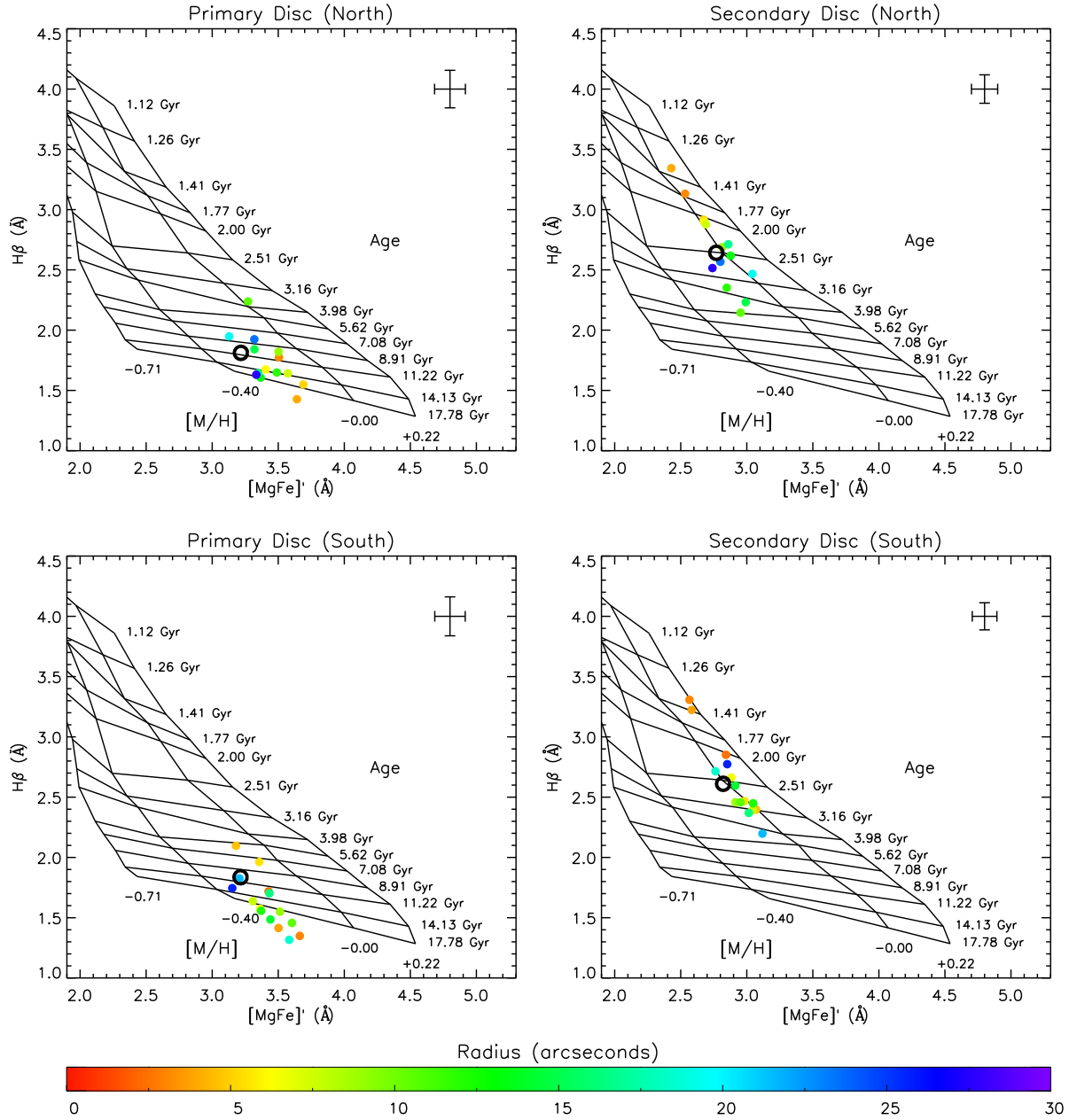


**Figure 3.** The line indices derived from the model components compared to the predictions of SSP models, measured out to a radius of  $\sim 30$  arcsec, or  $\sim 2.25$  kpc, where the S/N drops below 30 per Angstrom. The primary and secondary discs are in the left and right columns, while the north and south side of the galaxy are in the upper and lower rows. The radius of each measurement is color-coded; the open black points show the average value for the outer part of each disc. For clarity, points are plotted without errors; a typical error bar is shown in the top right of each plot.

of spectral classes, but found no significant systematic differences. Co-adding the data from the flat part of the rotation curve, we find a primary disc with a rotation velocity of  $143 \pm 7$  km s $^{-1}$  and a velocity dispersion of  $36 \pm 7$  km s $^{-1}$ , and a secondary disc with a lower rotation velocity of  $-118 \pm 8$  km s $^{-1}$  and a higher velocity dispersion of  $68 \pm 10$  km s $^{-1}$ , consistent with the previous findings of Rix et al. (1992).

There is clearly something a little strange about the kinematics derived for the emission-line gas disc. Because the gas shows a lower velocity dispersion than the secondary stellar disc that co-rotates with it, one would expect it to display a smaller amount of

asymmetric drift, and hence rotate more quickly, whereas it actually rotates slower than the accompanying stars. This strange property does not seem to be the result of any failing in extracting the gas kinematics correctly: we can obtain some confidence that the fitting process is picking up the correct properties for the hydrogen emission lines by comparing the results obtained to those measured directly from the excluded [OIII] $_{\lambda 5007}$  line, also shown in Figure 2, which are clearly very similar. The most likely explanation is therefore that the gas does not form a simple equilibrium axisymmetric disc, and hence would not obey the usual asymmetric drift equation. Some indication of an asymmetry in the [OIII] gas velocity



with respect to the projected major axis, is visible in Sarzi et al. (2006).

#### 4 STELLAR POPULATIONS

Having kinematically decomposed the spectra into the two stellar disc components at each radius, we can now study the stellar populations of each individual component, as derived from the strengths of its absorption lines. In order to render the line strengths at different radii comparable, all component spectra were broadened with Gaussians to match their dispersions to the largest values found at the centre of the galaxy. The  $H\beta$ , Mgb, Fe5270 and Fe5335 indices were then measured using the INDEXF package<sup>2</sup>. This software uses the Lick/IDS index definitions to calculate a pseudo-continuum over each absorption feature based on the level of the spectrum in bands on either side, and measures the strength of the feature relative to the pseudo-continuum (Worthey et al. 1994; Worthey & Ottaviani 1997). The combined metallicity index,  $[MgFe]'$  (González 1993; Thomas, Maraston & Bender 2003), was then determined from these values. The uncertainty in each measurement was estimated from the propagation of random errors and the effect of uncertainties in the radial velocity.

Figure 3 shows the resulting values of the  $H\beta$  index, as an indicator of stellar population age, plotted against the  $[MgFe]'$  index, as an indicator of metallicity, for each component as a function of radius. We also show the average results obtained by combining all the outer disc data from the flat part of the rotation curve, as delineated in Figure 2. Since we have observations of both sides of the galaxy, in which the counter-rotating components will be Doppler shifted in opposite directions, we obtain two independent measurements of these quantities with potentially different systematic biases as different spectral features in the two components will end up superimposed in the composite spectra from each side. The good agreement between the two rows of plots shown in Fig. 3 again provides some confidence in the results. What is most striking about these plots is the systematic difference between the  $H\beta$  indices between the two components. In addition, there seems to be a fairly strong gradient in the  $H\beta$  index of the secondary component, with the largest values at the smallest radii.

The  $H\beta$  index is largely a measure of the age of the stellar population, and we can quantify what the differences mean by calculating simple stellar population (SSP) models for comparison with the data. Here, we have used the web interface<sup>3</sup> to the models of Vazdekis et al. (2010), which use the MILES stellar library (Sánchez-Blázquez et al. 2006), and degrade the library spectra to match the resolution of the data by convolving them with a Gaussian of the appropriate dispersion. In this way, we can obtain estimates of the relative ages and metallicities without the potential loss of information that would normally result from degrading the galaxy spectra and models right down to the resolution of the Lick indices. Figure 3 shows the line indices for the resulting grid of models of different ages and metallicities. Although the usual caveats apply to the absolute values of physical parameters derived from such analyses, it is clear that the two discs have systematically different age properties. In particular, the primary disc is old, with an age inferred here of  $\sim 11$  Gyr, while the secondary disc, which rotates in the same direction as the gas, is much younger at

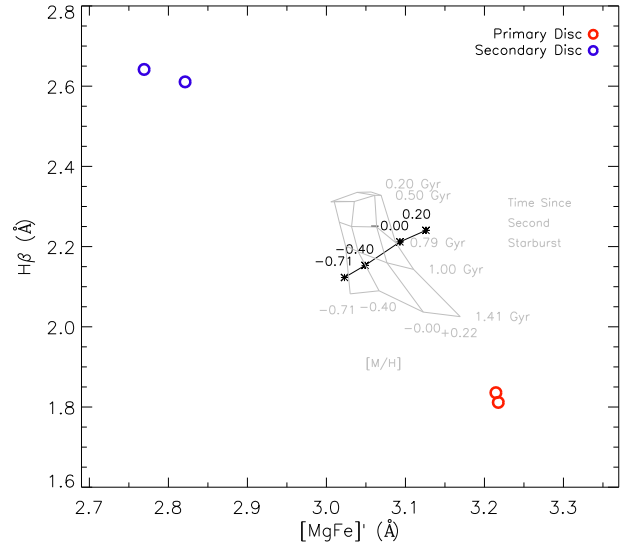


**Figure 4.** Model line indices derived for different star formation histories following separatrix crossing. The black line shows the effect on the line indices of the primary disc if the initial population had continuous steady star formation of differing metallicities until the present day, while the grey grid shows the effect of a single burst of star formation at the times and metallicities indicated. The open circles are the results for the two sides of the primary and secondary discs from Fig. 3.

$\sim 2.5$  Gyr, with its innermost parts even more youthful. Interestingly the young component also co-rotates with the molecular gas (Crocker et al. 2009), which is generally associated to recent star formation episodes.

#### 5 DISCUSSION AND CONCLUSIONS

By carefully disentangling the spectral components of NGC 4550, we have been able to learn a great deal about their individual properties, determining quantities that have significant implications for how this peculiar system might have formed. In particular, the strong differences in the stellar populations of the two discs seem to rule out the separatrix-crossing model in which they were formed from a single parent stellar population. It is interesting that one of the things that motivated Evans & Collett (1994) to consider this model in the first place was the apparent similarity of line strengths between components; as we have now seen, this similarity in apparent  $H\beta$  line strengths arises from an unfortunate cancellation between the stronger absorption lines of a younger population superimposed on the emission lines from the gas that rotates in the same direction.

However, the very presence of this gas suggests that all may not be lost for the separatrix-crossing model. Perhaps this scenario did indeed occur, creating two initially-identical stellar discs. Subsequent accretion then created a gas disc rotating in the direction of one of the stellar discs, and this gas then formed further generations of stars, creating a composite population in the disc co-rotating with the gas whose mean age would appear younger, as observed. Indeed, one could always invoke sufficient recent star formation to shift the inferred age from  $\sim 11$  Gyr to  $\sim 2.5$  Gyr. Since the line-index ages are effectively luminosity-weighted, a relatively modest amount of star formation, creating a bright young population, might explain the observed age differential.

<sup>2</sup> <http://www.ucm.es/info/Astrof/software/indexf/indexf.html>

<sup>3</sup> <http://miles.iac.es/>

Fortunately, we have one further constraint from this analysis that we can use to assess the viability of this modified scenario. Specifically, the decomposition of the spectra into the two stellar discs also tells us how much total light should be attributed to each component. Clearly, if one of the two initially-identical discs has had significant new stars forming in it, this component will have a greater luminosity. Encouragingly, this is what we find: the decomposition of the whole outer disc spectra (the open symbols in Figure 3) reveals that the secondary component, which co-rotates with the gas, has a continuum level at  $4400\text{\AA}$  (the centre of the B-band) that is 20% higher than the gas-free primary component.

So now we have an extra constraint which means that the amount of late star formation we can add is fixed by this additional 20% of B-band luminosity. We do not know the exact star formation history of any such late addition, but we can try out different possibilities. Figure 4 shows the results of such attempts again using the Vazdekis et al. (2010) models. The points at the bottom right show the line indices measured for the primary disc, which form the presumed starting point of the stellar population of both discs at the moment of separatrix crossing. The points at the top left show the higher indices that we are trying to reach by adding subsequent star formation. The line of crosses show what happens if we invoke continuous steady star formation of different metallicities ever since the old stellar population formed: the level of this star formation is then uniquely fixed by the requirement that its addition results in an enhancement of the disc's total B-band luminosity by 20%. Similarly, the grid of points shows the change in line indices caused by the addition of a single burst of star formation of varying ages and metallicities, again with the amplitude of the burst tuned to match the enhanced total luminosity of the disc. Since these two extreme possibilities of star formation history move the disc to the same region of the plot, it is not surprising that other more complicated possibilities also all end up in the same area. Clearly, although this additional later star formation moves the line indices in the right direction, it is nowhere near sufficient to reproduce the observed values for the younger disc.

With regret, we are therefore forced to abandon the elegance of the separatrix-crossing model entirely, and conclude that NGC 4550 formed through one of the other scenarios. The ages inferred in Section 4 then tell us something about the process. If formed through a carefully-controlled merger of fully-formed galaxies, these ages just reflect the ages of the progenitors. In the gas-rich accretion scenario, which now seems more natural, the  $\sim 2.5$  Gyr age of the secondary disc tells us how long ago this gas was accreted, with the residue of this accreted gaseous material still rotating along with this component, albeit in a somewhat non-circular manner. The higher velocity dispersion of this younger disc then presumably reflects the more turbulent nature of such secondary gas accretion when compared to the more conventional formation of the older primary stellar disc. We even begin to obtain some insight into the spatial distribution of this star formation, with the age gradient in the secondary component implying that the star formation has become ever more centrally concentrated as the gas has been depleted. If this scenario is correct, the only unexplained phenomenon is why the two counter-rotating disc components have such similar spatial extents, which at this point we must simply attribute to coincidence.

## ACKNOWLEDGEMENTS

We would like to thank Bruno Rodriguez del Pino for his help in debugging the modified code and for several useful discussions. We would also like to thank the anonymous referee for their useful comments that helped improve this paper. This work was based on observations obtained at the Gemini Observatory, which is operated by the Association of Universities for Research in Astronomy, Inc., under a cooperative agreement with the NSF on behalf of the Gemini partnership: the National Science Foundation (United States), the Science and Technology Facilities Council (United Kingdom), the National Research Council (Canada), CONICYT (Chile), the Australian Research Council (Australia), Ministério da Ciência, Tecnologia e Inovação (Brazil) and Ministerio de Ciencia, Tecnología e Innovación Productiva (Argentina). The programme IDs were GN-2009A-Q-102 and GS-2010A-Q-23. EJ acknowledges support from STFC, and MC acknowledges support from a Royal Society University Research Fellowship

## REFERENCES

- Bertola F., Buson L. M., Zeilinger W. W., 1992, *ApJ*, 401, L79
- Cappellari M., Emsellem E., 2004, *PASP*, 116, 138
- Cappellari M. et al., 2007, *MNRAS*, 379, 418
- Cappellari M. et al., 2011, *MNRAS*, 413, 813
- Coccato L., Morelli L., Corsini E. M., Buson L., Pizzella A., Vergani D., Bertola F., 2011, *MNRAS*, 412, L113
- Crocker A. F., Jeong H., Komugi S., Combes F., Bureau M., Young L. M., Yi S., 2009, *MNRAS*, 393, 1255
- Evans N. W., Collett J. L., 1994, *ApJ*, 420, L67
- González J. J., 1993, PhD thesis, Univ. California, Santa Cruz
- Krajnović D. et al., 2011, *MNRAS*, 414, 2923
- Kuijken K., Fisher D., Merrifield M. R., 1996, *MNRAS*, 283, 543
- Mei S. et al., 2007, *ApJ*, 655, 144
- Prugniel P., Soubiran C., 2001, *A&A*, 369, 1048
- Puerari I., Pfenniger D., 2001, *Ap&SS*, 276, 909
- Reynolds C. S., Ward M. J., Fabian A. C., Celotti A., 1997, *MNRAS*, 291, 403
- Rix H.-W., Franx M., Fisher D., Illingworth G., 1992, *ApJ*, 400, L5
- Rubin V. C., Graham J. A., Kenney J. D. P., 1992, *ApJ*, 394, L9
- Sánchez-Blázquez P. et al., 2006, *MNRAS*, 371, 703
- Sarzi M. et al., 2006, *MNRAS*, 366, 1151
- Thakar A. R., Ryden B. S., 1996, *ApJ*, 461, 55
- Thakar A. R., Ryden B. S., 1998, *ApJ*, 506, 93
- Thomas D., Maraston C., Bender R., 2003, *MNRAS*, 339, 897
- Toomre A., 1977, in *Evolution of Galaxies and Stellar Populations*, Tinsley B. M., Larson D. Campbell R. B. G., eds., p. 401
- Vazdekis A., Sánchez-Blázquez P., Falcón-Barroso J., Cenarro A. J., Beasley M. A., Cardiel N., Gorgas J., Peletier R. F., 2010, *MNRAS*, 404, 1639
- Worthey G., Faber S. M., González J. J., Burstein D., 1994, *ApJS*, 94, 687
- Worthey G., Ottaviani D. L., 1997, *ApJS*, 111, 377